
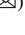






Influence of Viscosity on Density-Unstable Fluid-Fluid Displacement in Inclined Eccentric Annuli

Maryam Ghorbani¹  , Knut Erik Teigen Giljarhus² ,
and Hans Joakim Skadsem¹ 

¹ Department of Energy and Petroleum Technology, University of Stavanger, Stavanger, Norway
maryam.ghorbani@uis.no

² Department of Mechanical and Structural Engineering and Materials Science, University of Stavanger, Stavanger, Norway

Abstract. Construction of wells for oil production, geothermal energy recovery or geological storage of carbon dioxide is performed in stages by drilling the rock formation to a certain vertical depth, and then isolating the drilled section by running and cementing a casing string in the hole. The conventional cementing strategy relies on displacing the annular space behind the casing from the bottom and toward the surface. The conventional circulation direction therefore places the denser cementing fluids below the original annular fluid. An alternative cement placement strategy is to displace the annular space from the surface and downward by injecting cementing fluids directly into the annulus. Such reverse circulation operations have the benefit of lower circulation pressures and a reduced risk of fracturing the formation during placement, but also leads to density-unstable displacement conditions and increased risk of fluid contamination. To better understand how the design of cementing fluids and their placement rate affect reverse circulation displacements, we performed a series of computational simulations of density-unstable displacements using a realistic three-dimensional geometrical model of a wellbore annulus. We address the effects of wellbore inclination and inner pipe eccentricity, with a particular focus on impacts of the fluid viscosity hierarchy on the annular displacement efficiency. Our results show that increasing the displaced fluid viscosity will act to suppress the tendency for buoyant backflow, while it can worsen displacement of the narrow side of the eccentric annulus. Transverse secondary flows, which are stronger in cases where the displaced fluid is less viscous, contribute to the displacement of the narrow, low side of the annulus. We also observe that increasing the imposed axial velocity will tend to stabilize the annular displacement and suppress backflow, in agreement with previous work for buoyant pipe displacements. The present computational study is a step toward understanding how buoyant, inertial, and viscous stresses affect density-unstable displacement flows for reverse circulation cementing.

Keywords: Density-unstable fluids displacement · Viscosity ratio · Eccentric annuli

1 Introduction

Density-unstable fluid-fluid displacement, where one fluid is displaced by a denser fluid, exists in many geophysical [1–4] and industrial processes such as well cementing within the petroleum industry [5]. In primary cementing, the drilling fluid is displaced from the annular space between the casing and the formation and replaced by a cement slurry. The displacement can be performed by either conventional circulation or by the reverse circulation method. In conventional circulation primary cementing, the cement slurry is pumped down the well inside the casing and then up the annulus from the bottom of the well. Reverse circulation primary cementing is an alternative method for establishing annulus cement where the cementing fluids are injected down the well directly in the annulus. Figure 1 illustrates the flow path for conventional and reverse cementing methods.

Since the cement slurry is normally denser than the drilling mud, fluid displacement by the reverse circulation method generally leads to density unstable configuration in the annulus behind casing, and consequently higher risk of fluid contamination. Benefits of the reverse circulation cementing method include a reduced equivalent circulation density during placement and the possibility for shorter slurry thickening times, which makes this placement technique preferable compared to the conventional circulation method in certain cases [6–8]. For instance, the lower circulation pressure associated with reverse circulation cementing is an advantage for cementing of wells across weak or depleted formations [7, 8].

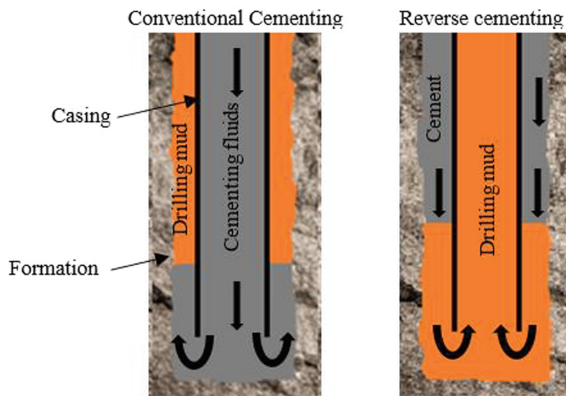


Fig. 1. Comparison of fluids displacement for a conventional and reverse circulation cementing. The cement is the displacing fluid, and the drilling fluid is the displaced fluid.

Once placed behind the casing, the cement slurry will harden to form an annular cement sheath that should seal the formation behind the casing and provide hydraulic isolation and mechanical support of the well. Isolation failure can lead to contamination of potable groundwater or leakage to the surface. Leakage can also compromise well productivity [5]. To successfully achieve hydraulic isolation outside the casing, the drilling fluid that occupies this annular space initially needs to be fully removed. Hence, investigation of the drilling fluid displacement has been motivation of several studies.

Annular fluid displacement is dependent on the geometry of the well and the annulus to be displaced. The annular space is often very narrow, and the casing is normally not perfectly centralized in the hole. Thus, casing eccentricity, which exists in most wells, will lead to non-uniform flow velocity over the annulus cross-section and promote an axial elongation of the interface between successive fluids during displacement. Drilling fluids, which are often yield stress fluids, can cease to flow altogether on the narrow side [9] or in parts of the annulus where the fluid velocity is low, such as inside a washed out section of the well [4, 10]. In an eccentric annulus, cement may favour the widest side and bypass slower-moving mud in the narrower side. The tendency of the cement to bypass the mud is a function of the geometry of the annulus, the density and viscosity of the mud and cement, and the imposed flow rate [11]. Tehrani et al. experimentally and theoretically studied the effect of eccentricity and flow rate and rig inclination on displacement efficiency for conventional circulation displacements. A positive effect on density stable displacement was found for increasing flow rates, while a negative effect was found for higher inclinations. However, the reduction of displacement efficiency can be compensated by careful selection of fluid rheology parameters [12, 13]. McLean et al. reported effects of buoyancy forces and rheological properties of mud and cement in the cementing process of an eccentric annulus [11]. Experimental studies of Malekmohammadi et al. in density stable displacement showed that small eccentricity, higher viscosity ratio, higher density ratio and slower flow rates all appeared to improve a steady displacement for Newtonian fluids and non-Newtonian fluids. However, the role of flow rate was less clear for non-Newtonian fluids.

The density unstable fluid configuration in reverse circulation cementing can result in Rayleigh-Taylor-like instabilities [14, 15] and increased intermixing between the fluids as a result. Séon et al. studied experimentally the buoyancy-driven exchange flow and the growth of the mixing region between two miscible fluids in a long pipe at different inclinations. The experiments showed that the mixing zone between the two fluids grows faster by increasing the inclination of the pipe up to an angle of 60° from the vertical direction. At higher inclinations, the greater transverse component of buoyancy leads to increased segregation and stratification of the fluids [16–18]. Etrati et al. performed a series of experiments to study the effect of viscosity ratio on the density-unstable fluid displacement in an inclined pipe. They found that increasing the viscosity of the displaced fluid destabilizes the flow and decreased the displacement efficiency [19]. Eslami et al. examined buoyant displacement flows in a vertical eccentric annulus experimentally. They demonstrated that there is higher level of instability and mixing between the fluids when the displaced fluid is more viscous than the displacing fluid. As a result, the fluid displacement was found less effective for these viscosity hierarchy configurations. A stronger effect of eccentricity on the fluid displacement was reported for viscoplastic fluids in comparison to Newtonian ones [20]. Skadsem and Kragset studied the buoyant displacement in a concentric vertical and inclined annulus using 3D numerical simulations [4]. The effect of imposed velocity was discussed and the importance of imposed flow rate and viscous stresses in suppressing the destabilizing effect of buoyancy were indicated.

Despite the aforementioned studies concerning density-unstable fluid displacement, reverse fluid displacement within the annular geometry is still relatively unexplored

from a computational point of view. In Skadsem and Kragset [4], the computational simulations were limited to iso-viscous fluids in a concentric annulus. In this paper we study the combined effect of eccentricity and viscosity ratio on the reverse fluid displacement in an annulus. Based on previous validation studies in buoyant exchange flows [21] and in reverse circulation displacement of iso-viscous miscible fluids [22], we limit the present study to computational simulations.

2 Geometry and Fluids

The geometry and fluids are chosen similar to Skadsem and Kragset [4], but now generalized to different eccentric orientations of the inner tube, and to Newtonian fluids with different viscosity ratios. The domain is a relatively narrow annulus with inner diameter (D_i) of 244.4 mm and the outer diameter (D_o) of 313.6 mm, giving a diameter ratio of 0.78. These dimensions correspond to the outer diameter of a 9 5/8-in production casing inside a typical 13 3/8-in intermediate casing, which are considered relevant for production wells in the North Sea [23].

In Skadsem and Kragset [4], the focus was on concentric and near-vertical annulus. Even if measures are taken in the field to centralize the casing within the wellbore, e.g. using bow-spring or rigid centralizers, the mechanical and hydraulic forces that act on the inner casing will normally de-centralize it in the wellbore [24, 25]. The annulus that is to be displaced to a cement slurry is therefore generally an eccentric annulus where fluids tend to move faster in the wider sector of the annulus. Further, with the exception of the very upper part of the wellbore, most of the deeper wellbore sections are drilled at an inclination from the vertical to optimize reservoir penetration and to enable production of remote areas far from existing infrastructure. To study the combined effects of eccentricity and inclination on the annular displacement, we consider inner casing eccentricities of 0.1, 0.3 and 0.7, and fix the inclination to 20° from vertical, with the narrow sector of the annulus to the low side. Regarding the properties of the fluids, we assume mass densities of 1820 kg/m^3 for the displaced fluid and 1900 kg/m^3 for the displacing fluid. These densities are realistic fluid densities based on industrial cementing properties [4, 23]. The corresponding Atwood number ($At = (\rho_H - \rho_L)/(\rho_H + \rho_L)$) is 0.022, where subscripts H and L denote heavy (displacing) and light (displaced) fluids, respectively. A constant viscosity of 0.1 Pa·s is assumed for the displacing fluid and values of 0.02, 0.1, 0.5 Pa·s are taken as the viscosity of the displaced fluid. The imposed bulk velocity of the fluid in the annulus is set to 0.44 m/s and 0.1 m/s. This corresponds to imposed flow rates of approximately 800 l/min and 182 l/min, respectively.

The problem outlined above is a density unstable displacement in an inclined eccentric annulus where the displacing fluid is injected from the top of the annulus at a constant imposed velocity. In the absence of interfacial tension between the fluids, and assuming smooth inner and outer casing surfaces (no wall surface roughness) the displacement problem may be characterized by the following 5 dimensionless numbers:

$$Re = \frac{\bar{\rho}V_0d}{\mu}, Fr = \frac{V_0}{\sqrt{Atgd}}, \beta, e = \frac{2\delta}{D_o - D_i}, m = \frac{\mu_L}{\mu_H}$$

Here V_0 is the imposed velocity, $d = (D_o - D_i)/2$ is the radial gap width of the annulus, $\bar{\rho}$ is the mean density of two fluids, g is the gravitational acceleration, β is the

inclination (from vertical reference line), δ and e are the casing deflection from the well centerline and the eccentricity of the annulus respectively. The mean viscosity of the fluids is denoted by $\bar{\mu}$, and μ_L and μ_H represent the viscosity of light and heavier fluid, respectively. The ratio of inertial to viscous forces is written as quantified by the Reynolds number, Re , and the ratio of mean-imposed velocity to an inertial-buoyant velocity scale, $V_I = \sqrt{Atgd}$, is the densimetric Froude number. The range of dimensionless numbers considered in this study are summarized in Table 1.

Table 1. Range of dimensionless numbers considered in the simulations.

Parameter	Value
Re	21.5, 64.5, 94, 107, 283, 471
Fr	1.15, 5.15
e	0.1, 0.3, 0.7
m	0.2, 1, 5
β	20°

3 Numerical Method

The fluid displacement in the annulus is simulated by OpenFOAM, version 2012, employing the twoLiquidMixingFoam solver, which is a solver for two-phase, incompressible, and miscible fluids. The concentration is evolved by a mixture fraction equation,

$$\frac{\partial \alpha}{\partial t} + \nabla \cdot (\alpha \mathbf{U}) = 0 \tag{1}$$

where α is the volumetric phase fraction of the displacing fluid. We assume molecular mixing between the fluids is negligible [26, 27].

The momentum and continuity equations are as follows:

$$\frac{\partial \rho \mathbf{U}}{\partial t} + \nabla \cdot (\rho \mathbf{U} \mathbf{U}) = -\nabla p + \nabla \cdot 2\mu \mathbf{S} + \rho \mathbf{g}, \tag{2}$$

$$\nabla \cdot \mathbf{U} = 0, \tag{3}$$

where $\mathbf{S} = [(\nabla \mathbf{U}) + (\nabla \mathbf{U})^T]/2$ is the rate of strain tensor, \mathbf{g} is the gravitational acceleration. The mixture fluid properties can be found from the phase fraction as

$$\rho = \alpha \rho_H + (1 - \alpha) \rho_L, \tag{4}$$

$$\mu = \alpha \mu_H + (1 - \alpha) \mu_L, \tag{5}$$

Here, μ is the mixture fluid viscosity and ρ is the mixture density.

Second order discretization schemes and a second order implicit scheme are employed for spatial terms and the time discretization, respectively. To stabilize the solution an adjustable time step with a maximum Courant number of 0.5 is used. For the boundary conditions, velocity Dirichlet conditions are prescribed at solid boundaries and at the inlet (no slip and uniform, and bulk inlet velocity, respectively) and a Neumann outflow condition at the outlet. For the pressure, Neumann inlet and Dirichlet outlet conditions are used.

A computational domain with 8 m length, equal to 116 hydraulic diameters, in the axial direction is used. The initial interface between the two fluids is located 2 m below the inlet at the top. The computational grid is a structured grid, stretched towards the walls and the eccentric side. The computational mesh consists of 160 grid cells in the azimuthal direction, 30 cells in the radial direction and 1024 cells in the axial direction. The computational grid for different eccentricities is shown in Fig. 2. A grid sensitivity study was performed to ensure the results were not significantly influenced by the chosen grid resolution, see Appendix 1.

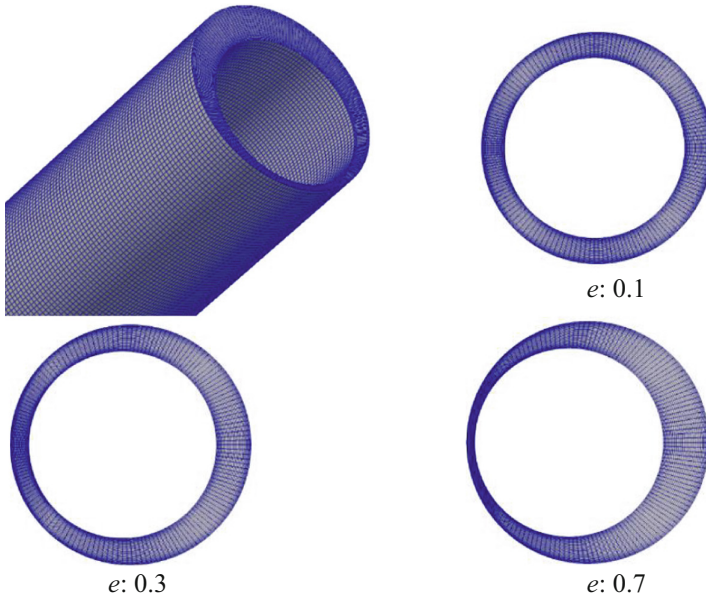


Fig. 2. The computational grid with different eccentricities

4 Results and Discussion

In the following sections, we present results from the 3D numerical simulations using different plotting techniques for studying and comparing how eccentricity, viscosity ratio and imposed flow rate affect the displacement. In addition to 3D renderings of

selected simulations, we also present results in the form of an “unwrapped” annulus where the fluid concentration is averaged across the radial gap, as shown in Fig. 3. For a given time in the simulation, this results in a 2D visualization of the displacement flow. Due to the inclination and the eccentricity, the fluid evolution is non-uniform over the annulus cross-section. Using the radially averaged concentration profiles, we plot the fluid concentration field in different azimuthal sides of the annulus, see Fig. 5 as an example. As indicated in Fig. 3, the letters “N”, “W” and “S” denote the narrow, wide, and lateral sides of the annulus, respectively and “Z” denotes the axial position. The outlet is taken at $Z = 0$ m, the inlet is at $Z = 8$ m, and the initial interface position is at $Z = 6$ m. Finally, we also present spatiotemporal diagrams, where the fluid concentration is averaged over the entire cross-section, and the resulting axial concentration profile is plotted as function of time since start of displacement. The spatiotemporal diagrams can be useful when comparing major features of the displacement cases and provide quantitative information about the extent and evolution of the fluid mixing zone.

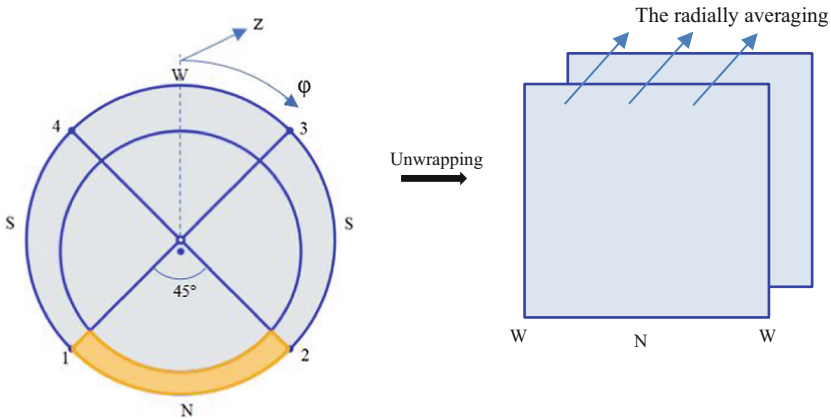


Fig. 3. Illustration of unwrapping and averaging procedure across the gap

4.1 Combined Effect of Imposed Velocity and Viscosity Ratio

Figure 4 compares the effect of the imposed velocity on the fluid displacement with different viscosity ratios using spatiotemporal diagrams. In the left column the displacing fluid is five times more viscous than the displaced fluid and vice versa in the right column. The imposed velocity in the plots in the second row is 4.4 times higher than plots in the first row. We define the mixing zone as the flow region where the concentration field, α , is between 0.01 and 0.99. In these plots the black dashed curves show the advancing front position during the displacement ($\alpha > 0.01$) while the light dashed curves show the rear, upper extent of the mixing zone ($\alpha < 0.99$). The local slope of the black dashed lines can be considered as the instantaneous front velocity, V_f .

As seen from the simulations with less viscous displaced fluid ($m = 0.2$), the tendency for backflow is prominent at the lowest imposed velocity, $Fr = 1.17$. As shown by the

white superimposed curve that tracks the rear edge of the mixing zone, some displaced fluid arrives above the initial interface position at $Z = 6$ m. This is referred to as *backflow* of displaced fluid. Backflow is associated with buoyant and unstable displacements, and result in rapidly growing mixing region. So, in this case ($Fr = 1.17$, $Re = 107$) the front velocity is higher than the case with viscosity ratio of 5 and the front position reaches the end of the annulus sooner at $t = 20$ s. We observe in Fig. 4 that backflow can be suppressed by either increasing the imposed velocity, and/or increasing the viscosity of the displaced fluid. At higher imposed velocity, $Fr = 5.15$, not only is there no backflow and slightly smaller front velocity, but there is also improved displacement of fluid at $m = 0.2$ compared to $m = 5$.

As reflected in the Reynolds number associated with these four spatiotemporal diagrams, increasing the viscosity of the displaced fluid (i.e., going from $m = 0.2$ to $m = 5$), results in a smaller Reynolds number. This is due to the Reynolds number being based on the *average* viscosity of the two fluids. Hence, by increasing the viscosity of the displaced fluid, leading to lower Re , the viscous forces suppress buoyancy, and there is no observable backflow at any of these flow rates. At the highest imposed flow rate ($Fr = 5.15$, $Re = 94.3$), the spatiotemporal diagram suggests reduced mixing between the fluids, and “stabilized” displacement where buoyancy is suppressed.

4.2 Combined Effect of Eccentricity and Viscosity Ratio

In a vertical and perfectly concentric annulus, there is no preferred direction for the dense, displacing fluid to flow since the driving forces (gravity and imposed flow) are parallel to the annulus axis, and the annular gap width is uniform. As mentioned in Sect. 2, the inner casing will in most practical cases be de-centralized inside the wellbore, and deeper well sections tend to be drilled at an inclination from the vertical direction. Inner-casing eccentricity will favor axial flow through the widest sector of the annulus, while gravity will promote flow of the denser fluid toward the low side of the annulus. In this section we will study the combined impact of inclination, eccentricity, and viscosity ratio on the fluid displacement for the case where the inner casing is offset toward the low side of the inclined wellbore.

Figure 5 presents gap-averaged concentration fields at initial stages of displacement, time = 6.6 s, for viscosity ratios of 0.2, 1 and 5 at eccentricity of 0.1, 0.3 and 0.7. By changing the viscosity of fluids, the preferred side of the annulus for the displacing fluid to flow in is also changed. Increasing the viscosity and the imposed velocity is seen to enhance the effect of eccentricity. In the cases with eccentricity of 0.1, at low imposed velocity, $Fr = 1.17$, the displacing fluid prefers the narrower side (Fig. 5a–c). For larger eccentricity, increasing the viscosity of the displaced fluid redirects the fluid to the wider regions; the lateral sides of the annulus (Fig. 5, e, h), or upper side (Fig. 5f, i). Increasing Fr strengthens the effect of eccentricity and the fluid flows in the wider side in most cases.

Figure 6 shows gap-averaged concentration fields at times that correspond to injection of equal volume of displacing fluid. The plots in the three columns on the left side correspond to the displacement with the velocity of 0.1 m/s and $Fr = 1.17$ at time of 20.6 s and the plots of the displacement with the higher velocity of 0.44 m/s and $Fr = 5.15$ at time of 5.6 s are shown on the right side. The highest level of instability, transverse

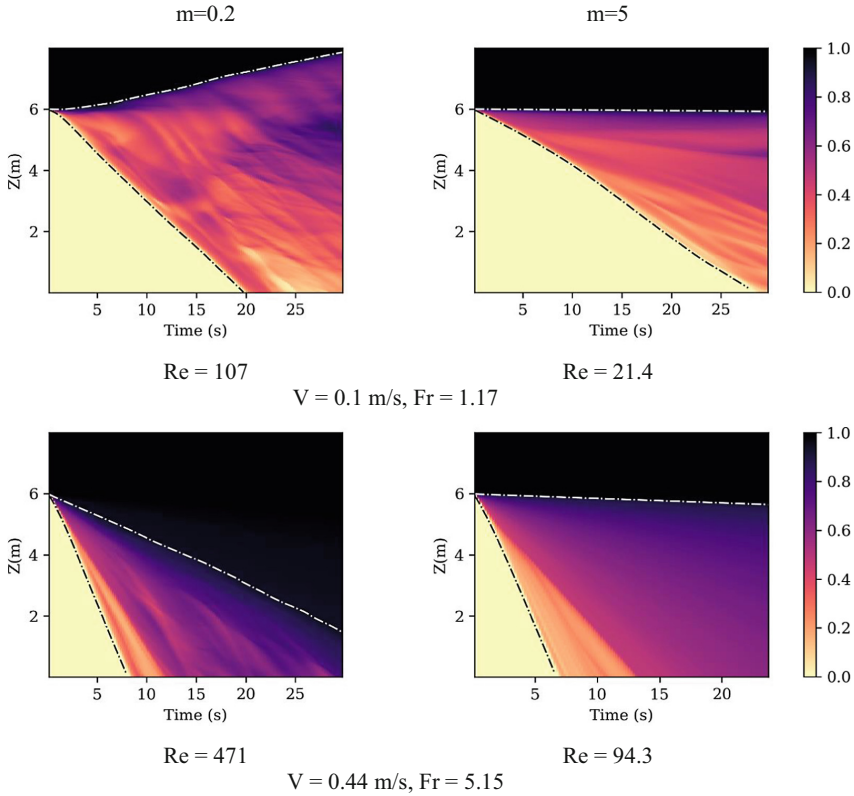


Fig. 4. Spatiotemporal diagrams for reverse circulation displacements in an inclined and eccentric annulus. The inclination is 20° and the eccentricity is 0.1

flow, and back flow of the lighter fluid are found for the cases with low imposed velocity and low viscous displaced fluid (Fig. 6 a, d, g). As discussed in Sect. 4.1, increasing the viscosity of the displaced fluid and imposed velocity tend to stabilize the displacement. It can be seen that there is less backflow in Fig. 6 (b, e, h) and no backflow for the viscous ratio of 5 in Fig. 6(c, f, i) and also more stable displacement is shown by imposing higher velocity Fig. 6 (right panels, $Fr = 5.15$).

To have a view on evolution of the mixing zone over the time of displacement the spatiotemporal diagrams from the simulations with viscosity ratios of 0.2 and 5 are presented in Fig. 7 at imposed velocity of 0.1 m/s and Fig. 8 at imposed velocity of 0.44 m/s. Cases with more viscous displaced fluid and higher imposed velocity correspond to more stable displacements, and spatiotemporal diagrams with smoother transitions across the mixing zone (Fig. 8-right column). However, this does not necessarily result in more effective displacement. According to Fig. 6, the displacement along the narrow side of the annulus is reduced as the displaced fluid viscosity increases. At $m = 5$, the resistance to flow along the narrower side of the annulus for the displaced fluid is stronger than it is at $m = 0.2$ and $m = 1$; this results in reduced displacement efficiency on the narrow side and a redirection of the flow toward the wider side.

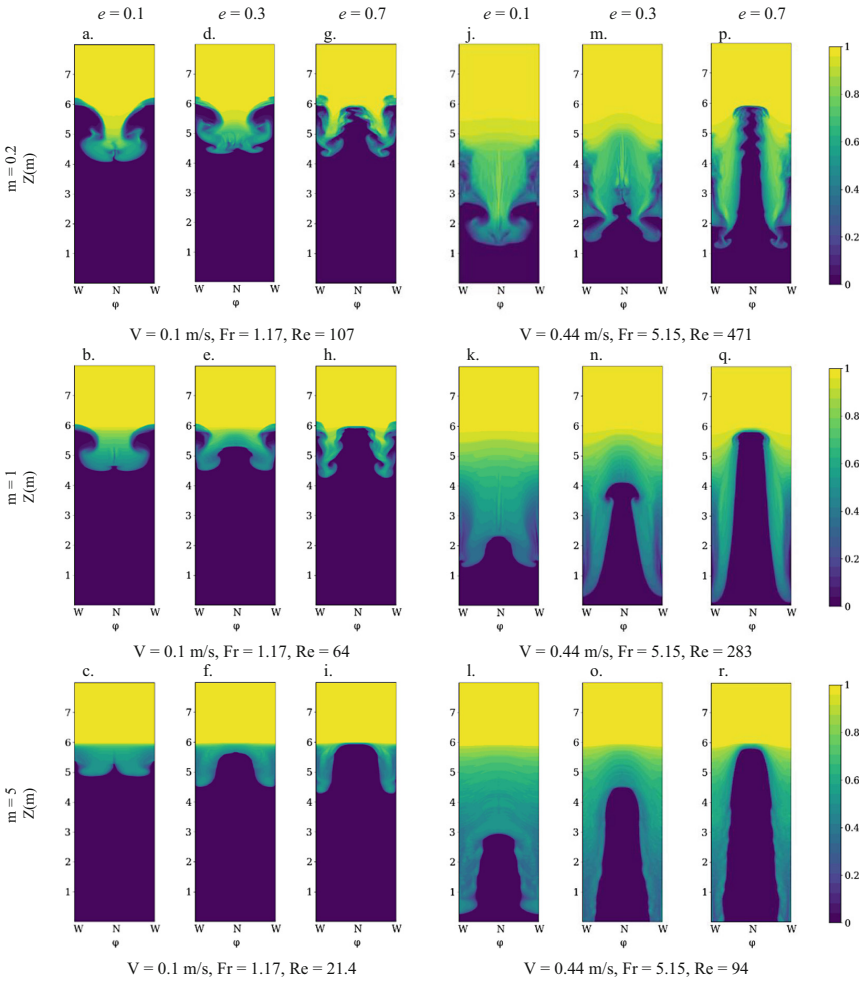


Fig. 5. The fluid concentrations averaged across the annular gap, at time 6.6 s

In Fig. 8, the dashed white line shows the front position in the *narrow* side of the annulus. By increasing the viscosity ratio, the slope of this line decreases meaning that the front velocity in this region decreases. The horizontal dashed white line in Fig. 8 at $e = 0.7$ and $m = 5$ indicates that there is no movement of the fluid-fluid interface at the narrow side of the annulus.

To do a quantitative study of the combined effect of eccentricity and viscosity ratio on the front velocity of the mixing region, V_f , the calculated front velocities are normalized by the imposed velocity, V_o , and plotted in Fig. 9 against eccentricity for all values of m and V_o . Figure 9 makes it clear that there is a different trend for the combined effect of eccentricity and viscosity ratio on the front velocity at $V_o = 0.1$ m/s ($Fr = 1.17$) and $V_o = 0.44$ m/s ($Fr = 5.15$). At $Fr = 5.15$ increasing the viscosity of the displaced fluid results in higher front velocity, while at $Fr = 1.17$, for $m = 0.2$ the front velocity is the highest.

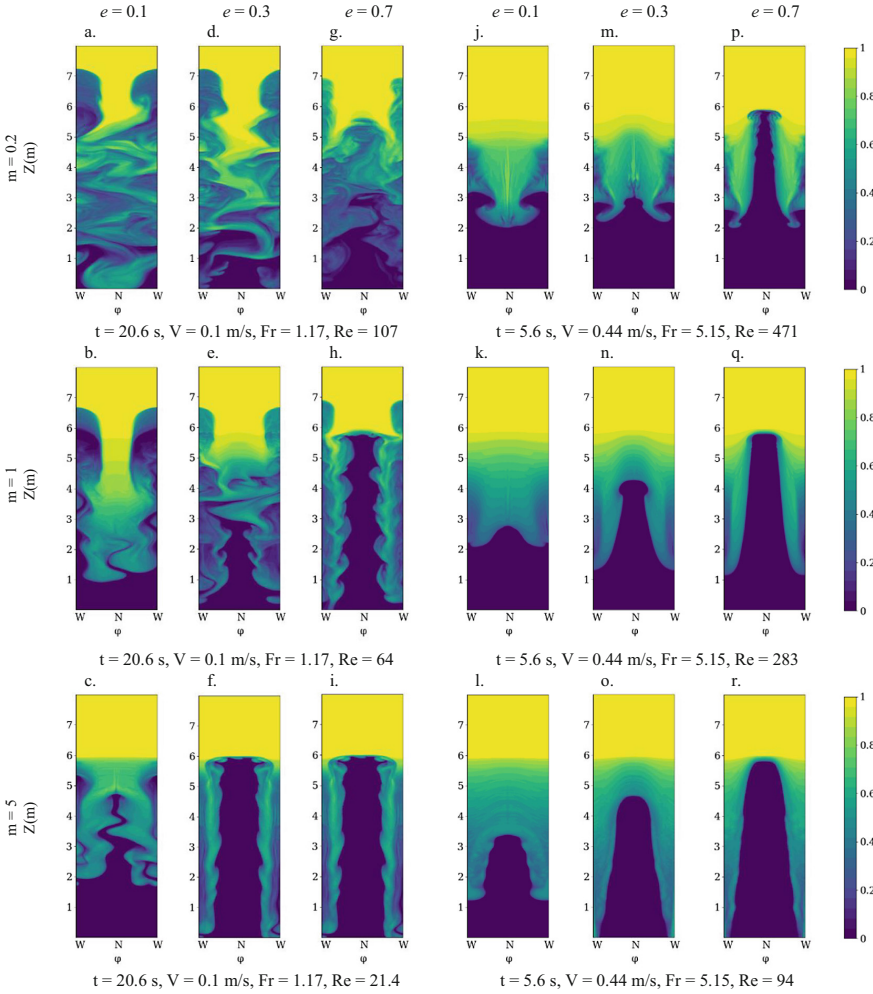


Fig. 6. The fluid concentrations averaged across the annular gap after imposing the same amount of displacing fluid.

The weaker impact of eccentricity for $m = 0.2$ and stronger effect of eccentricity for higher viscosity ratios can also be observed. The case that corresponds to the smallest normalized front velocity at the considered eccentricities is $m = 0.2$ and $V_0 = 0.44$ m/s. Since the displacements are subject to a constant imposed injection rate at the top, the smaller normalized front velocity suggests more effective displacement for this case ($m = 0.2$ and $V_0 = 0.44$ m/s) compared to the other cases considered.

4.3 Displacement in the Narrow Side

As discussed in the previous sections, the fluid prefers the wider side to flow in, so the displacement along the narrower side is often more challenging. Figure 10 compares

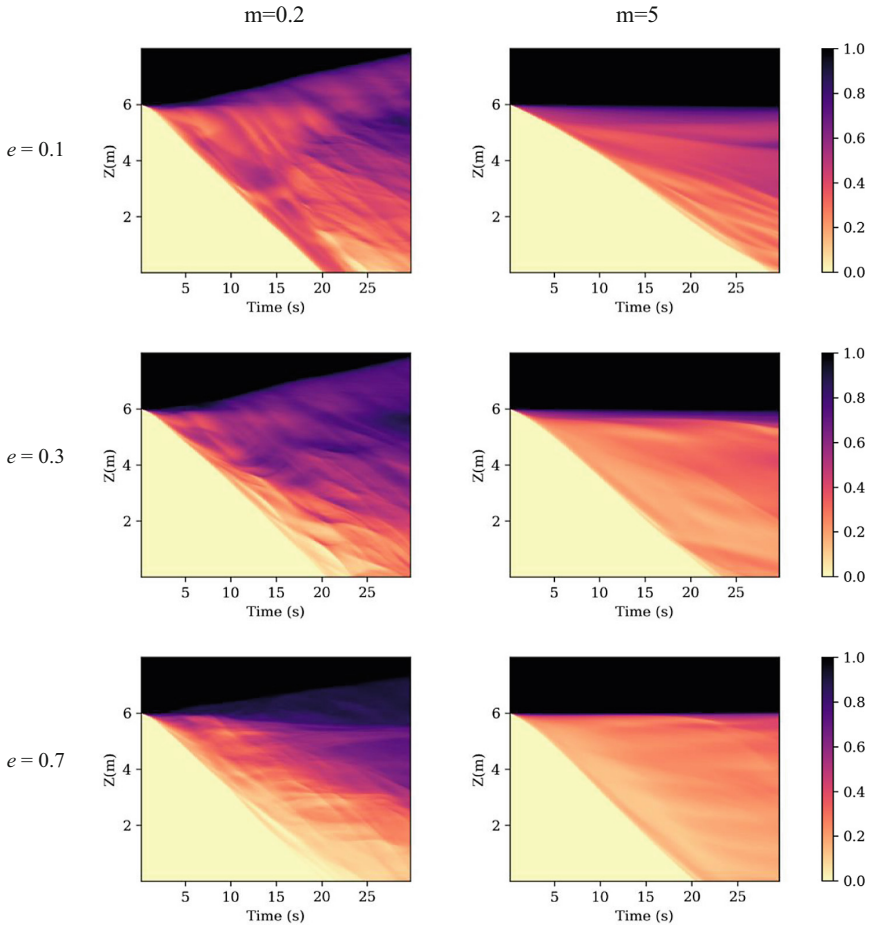


Fig. 7. Spatiotemporal diagrams for reverse circulation displacements in an inclined and eccentric annulus. The inclination is 20° and $V_o = 0.1$ m/s

the fluid concentration fields in the highly eccentric ($e = 0.7$) inclined annulus after imposing equal amount of displacing fluid at the two different velocities ($V_0 = 0.1$ m/s and time = 29.6 s in (a, b), $V_0 = 0.44$ m/s and time = 9.6 s in (c, d)). The left most diagrams (a, c) correspond to the cases with viscosity ratio of 0.2 and the other ones show the results of viscosity ratio of 5.

Further, Fig. 11 shows results from 3D simulation at different times for the highly eccentric and inclined annulus at the velocity of 0.44 m/s. The left panels correspond to $m = 0.2$ and the right panels to $m = 5$. As seen in Figs. 10 and 11, the greater viscosity in the displaced fluid ($m = 5$) results in higher restriction along the narrow/low side, and this negatively impacts the displacement here. In the cases with low viscosity displaced fluid, the displacement in the narrow side is facilitated by stronger transverse flow. In Fig. 11, we can see when the fluid cannot flow in the lower/narrower side at $m = 5$, the

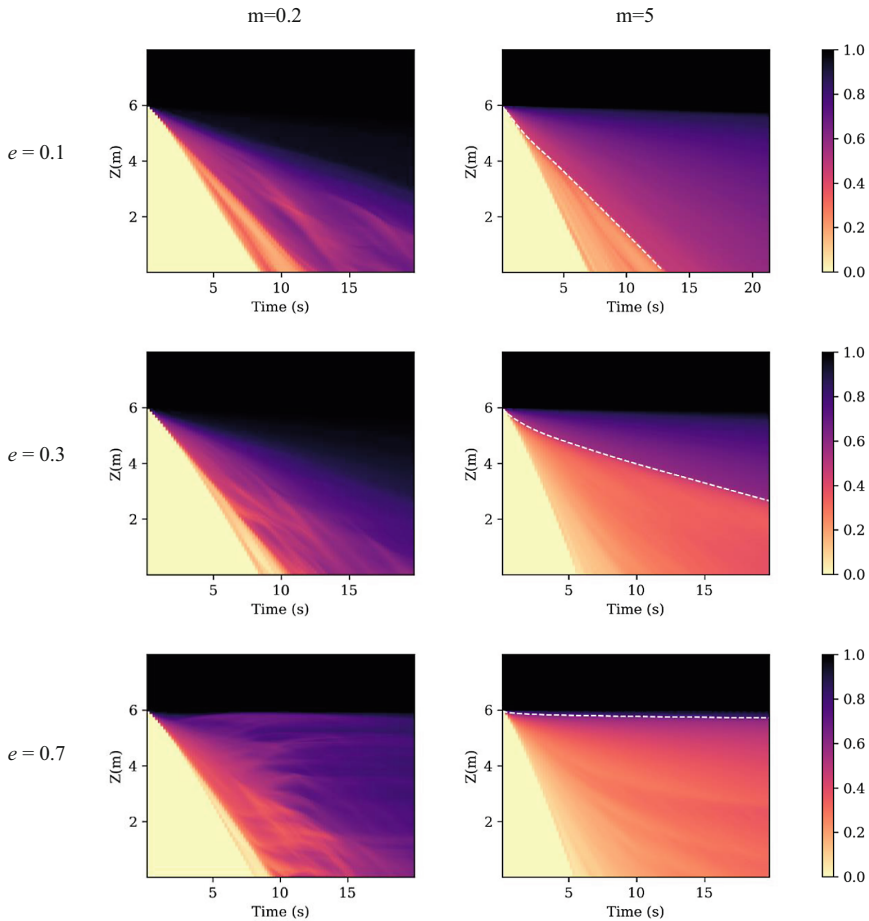


Fig. 8. Spatiotemporal diagrams for reverse circulation displacements in an inclined and eccentric annulus. The inclination is 20° and $V_o = 0.44$ m/s. The white dashed line represents the front position in the narrower side.

fluid flow in the upper/wider side with a higher velocity in comparison to the case with $m = 0.2$.

To have a better quantitative view on the combined effect of eccentricity and viscosity ratio on the displacement, the displacement efficiency in the narrow side of annulus (the orange section, N, in Fig. 3) is studied separately. In Fig. 12, the fluid displacement efficiency along this side is plotted versus time. The displacement efficiency at a given time corresponds to the volume fraction of displacing fluid along the narrow side. In these plots the results of the displacement with different viscosity ratios in the annulus with the eccentricities of 0.1, 0.3 and 0.7 are given. The imposed velocity for these cases is 0.44 m/s. It is shown that for each eccentricity, the most efficient displacement in the narrow side is when the displaced fluid is less viscous than the displacing fluid ($m = 0.2$). This observation agrees with the assessment of the normalized front velocity in

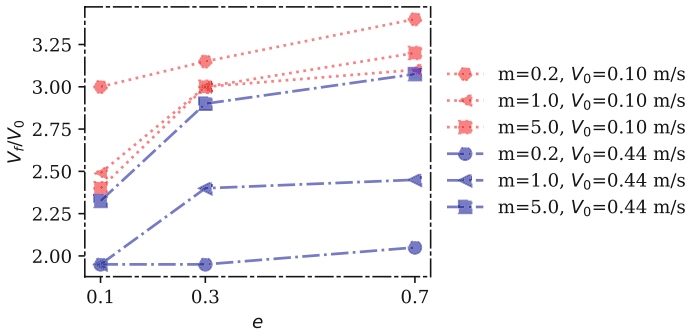


Fig. 9. Front velocity, V_f , normalized by imposed velocity, V_0 , for different eccentricity, e .

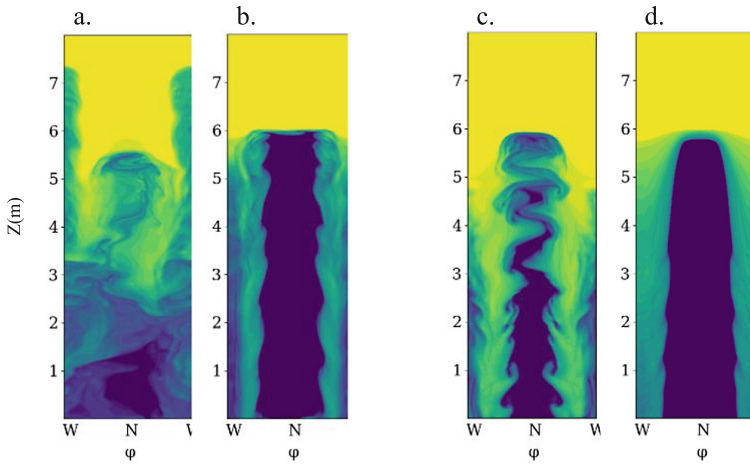


Fig. 10. The fluid concentrations averaged across the annular gap after imposing the same amount of displacing fluid, $e = 0.7$ and the imposed velocity for the two left plots is 0.1 m/s and $t = 29.6 \text{ s}$, and for the plots on the right side $V_0 = 0.44 \text{ m/s}$ and $t = 9.6 \text{ s}$.

Fig. 9. By increasing the eccentricity, the effect of viscosity ratio is strengthened, as by tracking the curves in the plots from left to right, it can be seen the difference between them increases.

5 Summary and Conclusion

Using 3D numerical simulations, we have investigated density-unstable displacement flows of Newtonian miscible fluids in an inclined annulus with different eccentricities. The study was motivated by so-called reverse circulation primary cementing of casing strings in wells but is also considered relevant for other industrial processes involving annular flow of two or more fluids. Our results have shown backflow and the highest level of instability at low imposed velocity for the case with less viscous displaced

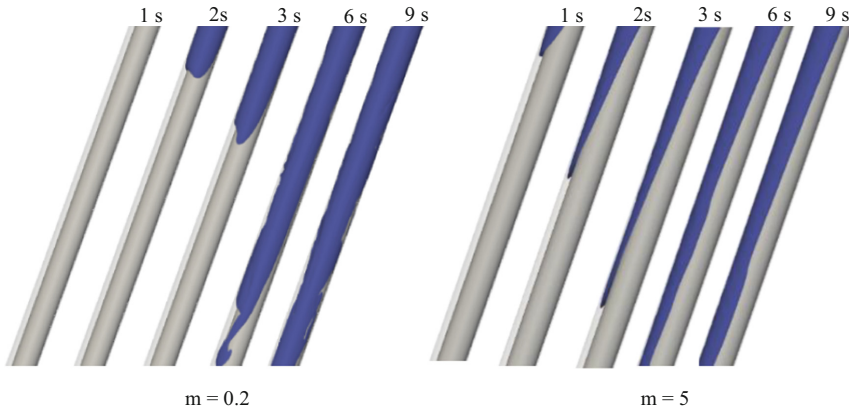


Fig. 11. 3D isocontour showing the displacing fluid for the highly eccentric and inclined annulus, $V_0 = 0.44$ m/s

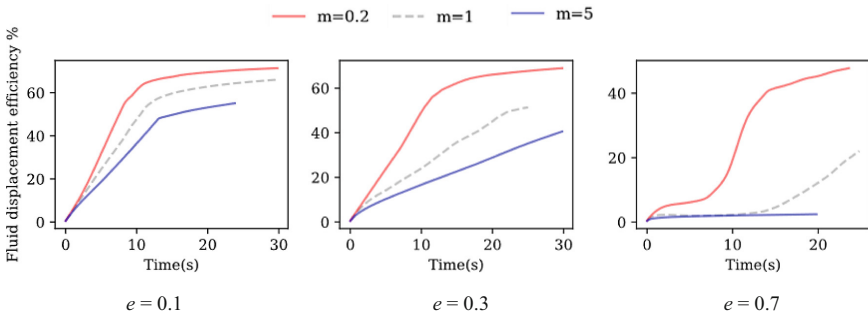


Fig. 12. The fluid displacement efficiency in the lower/narrower side of the annulus for imposed velocity $V_0 = 0.44$ m/s.

fluid. Increasing velocity can suppress this instability and results in more effective displacement. Increasing viscosity of the displaced fluid is also helpful for suppressing the backflow, but it does not necessarily lead to better fluid displacement.

The fluid evolution over the cross section of the annulus is uniform for a concentric vertical annulus. Eccentricity and/or inclination breaks this geometric symmetry and tend to promote displacement along either the wide or the narrow side of the annulus. The fluid prefers the wider side in an eccentric annulus, while gravity directs the denser fluid toward the lower side. Therefore, eccentricity and inclination can balance the effect of each other in cases where the narrow side of the annulus coincides with the low side. Our results have indicated that the fluid displacement in an eccentric annulus is not the same for all the viscosity ratios. When the displacing fluid is less viscous the fluid prefers the narrower/lower side at low imposed velocity and by increasing the eccentricity the fluid flows in the lateral sides. By increasing the viscosity of the displaced fluid, the effect of eccentricity becomes more significant, and the fluid is directed to the lateral

and wider sides at lower eccentricity. By imposing a higher imposed velocity, the effect of eccentricity becomes dominant, and the fluid prefer the wider/upper side to flow in.

We showed the effect of viscosity ratio on the front velocity is not the same at different Fr . At the low value of Fr , the highest front velocity is calculated for $m = 0.2$, while at the highest value of Fr the front velocity is higher at $m = 5$. The spatiotemporal plots have shown more stable pattern of the mixing zone at higher viscosity ratio. On the other hand, we discussed that for high eccentric annuli the instability exists at lower viscosity ratio is required, as these instabilities can facilitate the displacement on the narrower side.

In this study we studied the effect of viscosity ratio when the viscosity of the displaced fluid is constant which results in different value of mean viscosity. In future work, we will also investigate the effect of viscosity ratio at constant mean viscosity.

Appendix 1

We performed a grid sensitivity study to ensure the results were not significantly influenced by the chosen grid resolution. The simulation with parameters $Fr = 5.15$ and $Re = 283$ and an eccentricity of $e = 0.3$ was run with four different grid sizes, denoted coarse, medium, fine and extra fine. The total number of cells was doubled for each level, where fine corresponds to the grid resolution used in the remainder of the work.

Figure 13 shows the gap-averaged concentration field after 8 s. The overall evolution is almost identical for all resolutions, indicating that the fine resolution is satisfactory. This is further corroborated by the calculated front velocity and total displacement efficiency (ratio of displacing fluid volume and total annulus volume), which are shown in Fig. 14. Again, the results are not significantly influenced by the grid resolution.

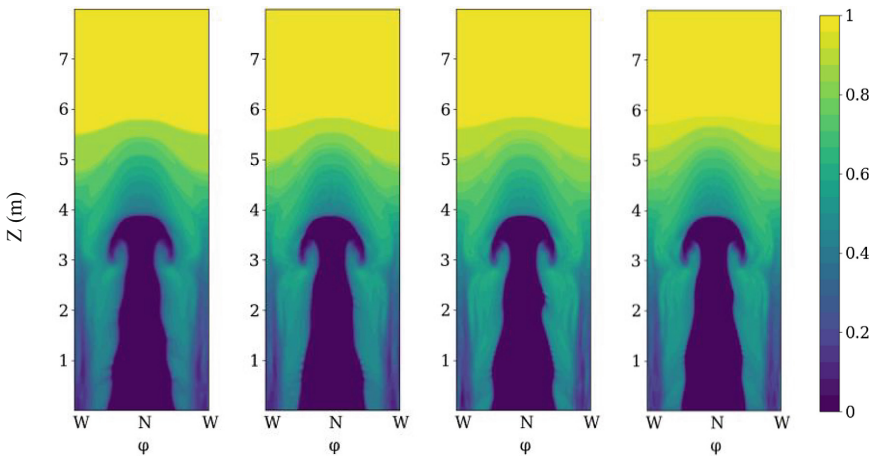


Fig. 13. Grid sensitivity study. Comparison of concentration field after 8 s. From left to right: Coarse, medium, fine, and extra fine.

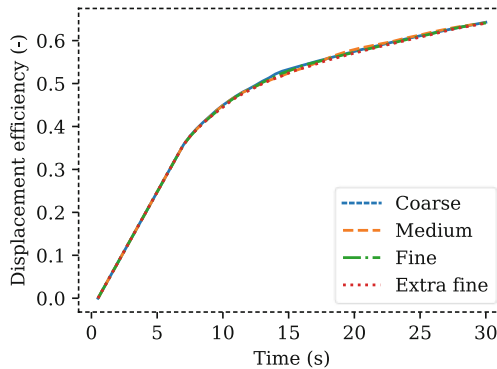


Fig. 14. Grid sensitivity study. Comparison of displacement efficiency for different grid sizes.

References

1. Benjamin, T.B., *Gravity currents and related phenomena*. Journal of Fluid Mechanics, 1968. **31**(2): p. 209-248.
2. Shin, J., S. Dalziel, and P. Linden, *Gravity currents produced by lock exchange*. Journal of Fluid Mechanics, 2004. **521**: p. 1-34.
3. Hallez, Y. and J. Magnaudet, *A numerical investigation of horizontal viscous gravity currents*. Journal of Fluid Mechanics, 2009. **630**: p. 71-91.
4. Skadsem, H. and S. Kragset, *A Numerical Study of Density-Unstable Reverse Circulation Displacement for Primary Cementing*. Journal of Energy Resources Technology, 2022. **144**.
5. Guillot, D. and E. Nelson, *Well cementing*. Schlumberger Educational Services, Sugar Land, TX, 2006.
6. McNerlin, B., et al. *Open Hole Fluid Displacement Analysis-Forward vs. Reverse Circulations*. in *SPE Annual Technical Conference and Exhibition*. 2013. OnePetro.
7. Macfarlan, K.H., et al., *A Comparative Hydraulic Analysis of Conventional-and Reverse-Circulation Primary Cementing in Offshore Wells*. SPE Drilling & Completion, 2017. **32**(01): p. 59-68.
8. Griffith, J., D. Nix, and G. Boe. *Reverse Circulation of Cement on Primary Jobs Increases Cement Column Height Across Weak Formations*. in *SPE Production Operations Symposium*. 1993. Society of Petroleum Engineers.
9. Walton, I. and S. Bittleston, *The axial flow of a Bingham plastic in a narrow eccentric annulus*. Journal of Fluid Mechanics, 1991. **222**: p. 39-60.
10. Roustaei, A. and I. Frigaard, *Residual drilling mud during conditioning of uneven boreholes in primary cementing. Part 2: Steady laminar inertial flows*. Journal of Non-Newtonian fluid mechanics, 2015. **226**: p. 1-15.
11. McLean, R., C. Manry, and W. Whitaker, *Displacement mechanics in primary cementing*. Journal of petroleum technology, 1967. **19**(02): p. 251-260.
12. Tehrani, A., J. Ferguson, and S. Bittleston. *Laminar displacement in annuli: a combined experimental and theoretical study*. in *SPE annual technical conference and exhibition*. 1992. OnePetro.
13. Tehrani, M., S. Bittleston, and P. Long, *Flow instabilities during annular displacement of one non-Newtonian fluid by another*. Experiments in Fluids, 1993. **14**(4): p. 246-256.
14. Drazin, P.G. and W.H. Reid, *Hydrodynamic stability*. 2004: Cambridge university press.
15. Sharp, D.H., *An overview of Rayleigh-Taylor instability*. Physica D: Nonlinear Phenomena, 1984. **12**(1-3): p. 3-18.

16. Séon, T., *Du mélange turbulent aux courants de gravité en géométrie confinée*. 2006, Université Pierre et Marie Curie-Paris VI.
17. Séon, T., et al., *Buoyancy driven miscible front dynamics in tilted tubes*. *Physics of fluids*, 2005. **17**(3): p. 031702.
18. Seon, T., et al., *Front dynamics and macroscopic diffusion in buoyant mixing in a tilted tube*. *Physics of Fluids*, 2007. **19**(12): p. 125105.
19. Etrati, A., K. Alba, and I.A. Frigaard, *Two-layer displacement flow of miscible fluids with viscosity ratio: Experiments*. *Physics of Fluids*, 2018. **30**(5): p. 052103.
20. Eslami, A., S. Akbari, and S. Taghavi, *An experimental study of displacement flows in stationary and moving annuli for reverse circulation cementing applications*. *Journal of Petroleum Science and Engineering*, 2022. **213**: p. 110321.
21. Ghorbani, M., et al. *Computational fluid dynamics simulation of buoyant mixing of miscible fluids in a tilted tube*. in *IOP Conference Series: Materials Science and Engineering*. 2021. IOP Publishing.
22. Ghorbani, M., A. Royaei, and H.J. Skadsem, *Reverse circulation displacement of miscible fluids for primary cementing*. *Journal of Energy Resources Technology*, 2023: p. 1–19.
23. Skadsem, H.J., et al., *Study of ultrasonic logs and seepage potential on sandwich sections retrieved from a North sea production well*. *SPE Drilling & Completion*, 2021. **36**(04): p. 976-990.
24. Gorokhova, L., A. Parry, and N. Flamant, *Comparing soft-string and stiff-string methods used to compute casing centralization*. *SPE Drilling & Completion*, 2014. **29**(01): p. 106-114.
25. McSpadden, A.R., O. Coker III, and G.C. Ruan, *Advanced casing design with finite-element model of effective dogleg severity, radial displacements, and bending loads*. *SPE Drilling & Completion*, 2012. **27**(03): p. 436-448.
26. Cook, A.W. and P.E. Dimotakis, *Transition stages of Rayleigh–Taylor instability between miscible fluids*. *Journal of Fluid Mechanics*, 2001. **443**: p. 69-99.
27. Hallez, Y. and J. Magnaudet, *Effects of channel geometry on buoyancy-driven mixing*. *Physics of fluids*, 2008. **20**(5): p. 053306.